An efficient kinetic modeling in plasmas relevant to inertial confinement fusion by using the AWBS transport equation

M. Holec,* V. Tikhonchuk, J.-L. Feugeas, and Ph. Nicolai
Centre Lasers Intenses et Applications, Universite de Bordeaux-CNRS-CEA, UMR 5107, F-33405 Talence, France.

P. Loiseau and A. Debayle
CEA, DAM, DIF, F-91297 Arpajon Cedex, France.

J. Brodrick and Ch. Ridgers
Plasma Institute, York, UK.

B. Dubroca
, Universite de Bordeaux, France.

R. Kingham
Imperial College, Lodon, UK.

(Dated: September 10, 2018)

Text of abstract.

I. INTRODUCTION

The first attempts of modern kinetic modeling of plasma can be tracked back to the fifties, when Cohen, Spitzer, and Routly (CSR) [1] demonstrated that the effect of Coulomb collisions between electrons and ions in the ionized gas predominantly results from frequently occurring events of cumulative small deflections rather than occasional close encounters. This effect was originally described by Jeans in [2] and Chandrasekhar [3] proposed to use the diffusion equation model of the Vlasov-Fokker-Planck type (VFP) [4].

A classical paper by Spitzer and Harm (SH) [5] provides the computation of the electron distribution function (EDF) in a plasma (from low to high Z) with a temperature gradient accounting for e-e and e-i collisions. The expressions for current and heat flux are widely used in every plasma hydrodynamic models. The distribution function based on the spherical harmonics method in its first approximation (P1) [6] is of the form $f^0+\mu f^1$, where f^0 and f^1 are isotropic and μ, is the direction cosine between the particle trajectory and some preferred direction in space. It should be emphasized that the SH solution expresses a small perturbation of equilibrium, i.e. that f^0 is the Maxwell-Boltzmann distribution and μf^1 represents a very small anisotropic deviation. This approximation holds for $L_T \gg \lambda_e$, a condition which is often invalid in laser plasmas, where L_T is the temperature length scale and λ_e the mean free path of electrons.

The actual cornerstone of the modern VFP simulations was set in place by Rosenbluth [7], when he derived a simplified form of the VFP equation for a finite expansion of the distribution function, where all the terms are computed according to plasma conditions, including f^0, which of course needs to tend to the Maxwell-Boltzmann distribution. Consequently, the pioneering work on numerical solution of the VFP equation [8, 9] revealed the importance of the nonlocal electron transport in laser-heated plasmas. In particular, that the heat flow down steep temperature gradients in unmagnetised plasma cannot be described by the classical, local fluid description of transport [5, 10]. This is due to the classical f^1 is not a small deviation (especially for electrons faster than thermal velocity), i.e. $f^0 \sim f^1$, since the nonlocal regime is characterized by $L_T \sim \lambda_e$. It was also shown that a thermal transport inhibition [8] on one hand side, and a nonlocal preheat on the other hand side, naturally appear. These effects are attributed to significant deviations of f^0 from Maxwellian distribution.

Nevertheless, numerical solution of the VFP equation even in the Rosenbluth formalism remains very challenging computationally, because the e-e collision integral is nonlinear. More simple linear forms of e-e collision operator are needed.

It is the purpose of this paper to present an efficient alternative to VFP model based on the Albritton-Williams-Bernstein-Swartz collision operator (AWBS) [11]. In Section II we propose a modified form of the AWBS collision operator, where its important properties are further presented in Section III with the emphasis on its comparison to the full VFP solution in local diffusive regime. Sec-

* milan.holec@u-bordeaux.fr

tion IV focuses on the performance of the AWBS transport equation model compared to modern kinetic codes including VFP codes Aladin and Impact [12], and PIC code Calder [13], where the cases related to real laser generated plasma conditions are studied. Finally, the most important outcomes of our research are concluded in Section V.

II. THE AWBS KINETIC MODEL

The electrons in plasma can be modeled by the deterministic Vlasov model of charged particles

$$\frac{\partial f}{\partial t} + \boldsymbol{v}\cdot\nabla_{\boldsymbol{x}} f + \frac{q_e}{m_e}\boldsymbol{E}\cdot\nabla_{\boldsymbol{v}} f = C_{ee}(f) + C_{ei}(f), \quad (1)$$

where $f(t,\boldsymbol{x},\boldsymbol{v})$ represents the density function of electrons at time t, spatial point $\boldsymbol{x}$, and velocity $\boldsymbol{v}$, and $\boldsymbol{E}$ is the electric field in plasma, q_e and m_e being the charge and mass of electron.

The general form of the e-e collision operator C_{ee} is the Fokker-Planck form published by Landau [14]

$$C_{FP}(f) = \Gamma \int \nabla_{\boldsymbol{v}}\nabla_{\boldsymbol{v}}(\boldsymbol{v}-\tilde{\boldsymbol{v}})\cdot(f\,\nabla_{\tilde{\boldsymbol{v}}} f - f\,\nabla_{\boldsymbol{v}} f)\,\mathrm{d}\tilde{\boldsymbol{v}}, \quad (2)$$

where $\Gamma = \frac{4\pi q_e^4 \ln\Lambda}{m_e^2}$ and $\ln\Lambda$ is the Coulomb logarithm. The e-i collision operator C_{ei} could be expressed in a simpler form since massive ions are considered to be motionless compared to electrons. The scattering operator accounts for the change of electron velocity without change in the velocity magnitude. It is expressed in spherical coordinates as

$$C_{ei}(f) = \frac{\nu_{ei}}{2}\left(\frac{\partial}{\partial\mu}\left((1-\mu^2)\frac{\partial f}{\partial\mu}\right) + \frac{1}{\sin^2\phi}\frac{\partial^2 f}{\partial\theta^2}\right), \quad (3)$$

where $\mu = \cos\phi$, ϕ and θ are the polar and azimuthal angles, and $\nu_{ei} = \frac{Z n_e \Gamma}{v^3}$ is the e-i collision frequency.

The e-e collision operator needs to be linearized for efficient computations. Fish introduced a linear form of C_{ee} in [15] in the high-velocity limit ($v \gg v_{th}$) electron collision operator

$$C_H(f) = v\nu_e\frac{\partial}{\partial v}\left(f + \frac{v_{th}^2}{v}\frac{\partial f}{\partial v}\right) + \frac{\nu_e}{2}\left(1 - \frac{v_{th}^2}{2v^2}\right)\left(\frac{\partial}{\partial\mu}\left((1-\mu^2)\frac{\partial f}{\partial\mu}\right) + \frac{1}{\sin^2\phi}\frac{\partial^2 f}{\partial\theta^2}\right), \quad (4)$$

where $\nu_e = \frac{n_e\Gamma}{v^3}$ is the e-e collision frequency and $v_{th} = \sqrt{\frac{k_B T_e}{m_e}}$ is the electron thermal velocity. The linear form of C_H arises from an assumption that the fast electrons predominantly interact with the thermal (slow) electrons, which simplifies importantly the form (2). However the diffusion term in the e-e collision operator (4) still presents numerical difficulties.

A yet simpler form of the collision operator of electrons was proposed in [16]

$$C_{AWBS}(f) = v\nu_e^*\frac{\partial}{\partial v}(f - f_M) + \frac{\nu_{ei}+\nu_e^*}{2}\left(\frac{\partial}{\partial\mu}\left((1-\mu^2)\frac{\partial f}{\partial\mu}\right) + \frac{1}{\sin^2\phi}\frac{\partial^2 f}{\partial\theta^2}\right), \quad (5)$$

where $f_M = \frac{n_e}{(2\pi)^{\frac{3}{2}} v_{th}^3}\exp\left(-\frac{v^2}{2v_{th}^2}\right)$ is the Maxwell-Boltzmann equilibrium distribution. Here, the first term representing the AWBS operator [11] accounts for relaxation to equilibrium due to the e-e collisions, and the second term accounts for the e-i and e-e collisions contribution to scattering.

A method of angular momenta for the solution of the electron kinetic equation with the collision operator (5) was introduced in [16, 17].

In (5) we have introduced a modified e-e collision frequency ν_e^* in order to address a proper behavior with respect to Z, which is further analyzed in Section III and promising results compared to the full FP operator are presented.

III. BGK, AWBS, AND FOKKER-PLANCK MODELS IN LOCAL DIFFUSIVE REGIME

An approximate solution to the so-called *local diffusive regime* of electron transport can be found, since the *diffusive regime* refers to a low anisotropy given by the projection μ. i.e. modeled by a simple P1 form of EDF

$$\tilde{f}(z,v,\mu) = f^0(z,v) + \mu f^1(z,v), \quad (6)$$

where z is the spatial coordinate along the axis z, v the magnitude of transport velocity, and $\mu = \cos\phi$, where ϕ is the pitch angle with respect to the axis z.

The approximate transport solution is then obtained when analyzing the action of the time-steady form of (1) in 1D on the approximation (6) as

$$\mu\left(\frac{\partial\tilde{f}}{\partial z} + \frac{q_e E_z}{m_e v}\frac{\partial\tilde{f}}{\partial v}\right) + \frac{q_e E_z}{m_e}\frac{(1-\mu^2)}{v^2}\frac{\partial\tilde{f}}{\partial\mu} = \frac{1}{v}C(\tilde{f}), \quad (7)$$

where C is a given collision operator including both e-e and e-i collisions.

The locality of transport is the best expressed in terms of the Knudsen number $Kn = \frac{\lambda}{L}$, where λ is the mean free path of electron and L the characteristic length scale of plasma. Consequently, plasma conditions characterized by $Kn \ll 1$ exhibit a local transport regime. This measure then play a very important role in our analysis, where we use the electroni-electron and electron-ion mean free paths $\lambda_e = Z\lambda_{ei} = \frac{v}{\nu_e}$, and the density and temperature plasma scale lengths $L_{n_e} = n_e/\frac{\partial n_e}{\partial z}$ and $L_{T_e} = T_e/\frac{\partial T_e}{\partial z}$.

A. The BGK local diffusive electron transport

Bhatnagar, Gross, and Krook introduced a very simple form of a collision operator [18]

$$C_{BGK}(\tilde{f}) = \nu_e(\tilde{f} - f_M) + \frac{\nu_{ei}+\nu_e}{2}\frac{\partial}{\partial\mu}(1-\mu^2)\frac{\partial\tilde{f}}{\partial\mu}. \quad (8)$$

In spite of its simple form, BGK collision operator (8) serves as a useful model providing a relevant kinetic response, yet only qualitative with respect to the FP collision operator (2). In particular, the conservation of kinetic energy, momentum, and number of particles is often violated [19].

However, the form of (8) provides a simple analytical treatment of local diffusive transport regime, when used in (7). As a result, one finds a simple form of the BGK isotropic and anisotropic terms of (6) to be

$$f^0 = f_M + Kn\frac{v_{th}^2}{v^2}f^1, \quad (9)$$

$$f^1 = -\frac{\lambda_e}{Z}\left(\frac{\partial f^0}{\partial z} + \frac{q_eE_z}{m_ev}\frac{\partial f^0}{\partial v}\right), \quad (10)$$

where $Kn = \frac{\lambda_e}{L_{n_e}} + \frac{5}{2}\frac{\lambda_e}{L_{T_e}}$ and a detailed derivation of (9) and (10) can be found in Appendix A. Equation (9) states that $f^0 \to f_M$ when $Kn \ll 1$, and accordingly, $f^1 \to -\frac{\lambda_e}{Z}\left(\frac{\partial f_M}{\partial z} + \frac{q_eE_z}{m_ev}\frac{\partial f_M}{\partial v}\right)$. When the quasi-neutrality constraint on the electric field (A7) is used, one finally obtains the analytical BGK form of (6)

$$\tilde{f}_{BGK} = f_M - \mu\left(\frac{v^2}{2v_{th}^2} - 4\right)\frac{1}{Z}\frac{\lambda_e}{L_{T_e}}f_M, \quad (11)$$

which recovers the Lorentz electron-ion collision gas model [20]. It should be noticed that f^0 equilibrates to f_M as $O(Kn^2)$ in (9), since $f^1 = \left(\frac{v^2}{2v_{th}^2} - 4\right)\frac{1}{Z}Knf_M$.

The details about the BGK distribution function compared to other collision operators can be found in Section III D.

B. The AWBS local diffusive electron transport

Similarly to the BGK model, the AWBS collision operator 5 explicitly uses equilibration to the Maxwell-Boltzmann distribution f_M. On the other hand side, AWBS originates from C_H, which is derived from the full FP operator (2). This makes the AWBS operator to be superior to the BGK operator, which is considered a pure phenomenological model.

If (5) is used in (7), one obtains the following equations governing the AWBS isotropic and anisotropic terms of (6)

$$\frac{\partial f^0}{\partial v} = \frac{\partial f_M}{\partial v} + Kn\frac{v_{th}^2}{v^2}\frac{f^1}{v}, \quad (12)$$

$$\frac{\partial f^1}{\partial v} - \frac{Z+1}{v}f^1 = \frac{\lambda_e}{v}\left(\frac{\partial f^0}{\partial z} + \frac{q_eE_z}{m_ev}\frac{\partial f^0}{\partial v}\right), \quad (13)$$

A detailed derivation of (12) and (13) can be found in Appendix A. One observes that f^0 goes to Maxwellian when the local regime of transport is settled. Indeed, according to equation (12) the derivative $\frac{\partial f^0}{\partial v} \to \frac{\partial f_M}{\partial v}$ when $Kn \ll 1$ for any electron velocity, thus leading to $f^0 \to f_M$. Consequently, one finds the AWBS model equation for f^1 in local diffusive regime to be

$$\frac{\partial f^1}{\partial v} + \frac{Z+1}{v}f^1 = \frac{\lambda_e}{v}\left(\frac{1}{L_{n_e}} + \left(\frac{v^2}{2v_{th}^2} - \frac{3}{2}\right)\frac{1}{L_{T_e}} - \frac{q_eE_z}{m_ev_{th}^2}\right)f_M. \quad (14)$$

Since there is no simple analytical formula for f^1 solving (14), we adopt the implicit Euler numerical integration with $\Delta v < 0$, i.e. we integrate from high electron velocity ($v_{max} = 7v_{th}$) to the velocity equal to zero (using 10^4 steps). This mimics a particle deceleration due to collisions. The correct numerical solution of (14) corresponds to an appropriate value of E_z leading to a zero current. Interestingly, this numerical value matches precisely the Spitzer electric field (A7).

As in the BGK case, the numerical solution of (14) reveals that $f^1 \sim Knf_M$ and that f^0 equilibrates to f_M as $O(Kn^2)$ based on (12).

The details about the AWBS distribution function compared to other collision operators can be found in Section III D.

C. The Fokker-Planck local diffusive electron transport

The solution to the 1D transport equation (7) using the Fokker-Planck collision operator (2) is very ambitious, as demonstrated in [1, 3, 7], fortunately, one can use the explicit evaluation of the electron distribution function published in [5], which takes the following form

$$f^1(z,v) = \frac{v_{2th}^4}{\Gamma Z n_e}\left(2\tilde{D}_T\left(\frac{v}{v_{2th}}\right) + \frac{3}{2}\frac{\gamma_T}{\gamma_E}\tilde{D}_E\left(\frac{v}{v_{2th}}\right)\right)\frac{f_M}{T}\frac{\partial T_e}{\partial z}, \quad (15)$$

where $\tilde{D}_T(x) = ZD_T(x)/B$, $\tilde{D}_E(x) = ZD_E(x)/A$, γ_T, and γ_E are numerical values in TABLE I, TABLE II, and TABLE III in [5], and $v_{2th} = \sqrt{\frac{k_BT_e}{2m_e}}$.

One should be aware, that the solution of (7) equipped with the full FP collision operator reveals the importance of e-e Coulomb collisions, which is emphasized in the Z dependence of the distribution function, current, heat flux, electric field, etc. In particular, the latter exhibits the following dependence [5]

$$\boldsymbol{E} = \frac{m_ev_{th}^2}{q_e}\left(\frac{\nabla n_e}{n_e} + \left(1 + \frac{3}{2}\frac{Z+0.477}{Z+2.15}\right)\frac{\nabla T_e}{T_e}\right), \quad (16)$$

which for $Z \gg 1$ corresponds to the classical Lorentz electric field (A7).

	$Z=1$	$Z=2$	$Z=4$	$Z=16$	$Z=116$
$\bar{\Delta}\boldsymbol{q}_{AWBS}$	0.057	0.004	0.038	0.049	0.004
$\phi(Z)$	-0.045	0.004	0.032	0.052	0.055

TABLE I. Relative error $\bar{\Delta}\boldsymbol{q}_{AWBS} = |\boldsymbol{q}_{AWBS} - \boldsymbol{q}_{SH}|/\boldsymbol{q}_{SH}$ of the $\nu_e^* = \frac{\nu_e}{2}$ scaling used in the AWBS model (5) showing the discrepancy (maximum around 6%) with respect to the original solution of the heat flux given by numerical solution in Spitzer and Harm [5]. The values of $\phi(Z)$ (weak dependence) are also shown.

D. Summary of the BGK, AWBS, and Fokker-Planck local diffusive transport

Ever since the SH paper [5], the effect of microscopic electron transport on the current $\int q_e \boldsymbol{v} \tilde{f}\, \mathrm{d}\boldsymbol{v}$ and the heat flux $\int \frac{m_e|\boldsymbol{v}|^2}{2}\boldsymbol{v}\tilde{f}\, \mathrm{d}\boldsymbol{v}$ in plasmas under local diffusive conditions has been understood. By overcoming some delicate aspects of the numerical solution to (2) presented in the CSR paper [1], the effect of electron-electron collisions was properly quantified and the correct dependence on Z of the heat flux $\boldsymbol{q}$ was approximated as [5, 21]

$$\boldsymbol{q} = \frac{Z+0.24}{Z+4.2}\boldsymbol{q}_L, \tag{17}$$

where $\boldsymbol{q}_L = \kappa T_e^{\frac{5}{2}} \nabla T_e$ is the heat flux given by Lorentz gas model [20]. In the case of the BGK operator and its EDF formula (11), the correct dependence on Zcan be simply achieved by scaling the e-e and e-i collision frequencies as

$$\nu_e^{BGK} = \frac{\nu_{ei}^{BGK}}{Z} = \frac{Z+4.2}{Z+0.24}\nu_e, \tag{18}$$

which imposes a right heat flux magnitude (17).

We have performed an extensive computational analysis in the case of the AWBS operator in order to obtain the heat flux behavior while varying Z. As expected, the heat flux magnitude did not match exactly the Z-dependence (17), e.g. for $Z=1$ the AWBS heat flux was about 60% less than the SH calculation, while there was a perfect match in the case of $Z \gg 1$. By assuming that the e-e collisions are responsible for this inadequacy, we searched for a scaling of ν_e in (5). Interestingly, we found an almost constant scaling, i.e. with a very weak dependency on Z as

$$\nu_e^* = \left(\frac{1}{2} + \phi(Z)\right)\nu_e \approx \frac{\nu_e}{2}, \tag{19}$$

where the actual dependence is $\phi(Z) \ll \frac{1}{2}$ for any Z. Indeed, TABLE I shows $\phi(Z)$ and its corresponding relative error (maximum around 6%) of the heat flux modeled by (5) vs. SH results represented by (17). It should be noted that the error is calculated with respect to original values presented in TABLE III in [5].

Nevertheless, the electron-electron collisions effect represented by (17) provides only an integrated information about the heat flux magnitude. If one takes a closure look at the distribution function itself, the conformity of the modified AWBS collision operator is even more emphasized as can be seen in FIG. 1 showing the flux moment in spherical coordinates of velocity $q_1 = \frac{m_e v^2}{2} v f^1 v^2$. In the case of the high Z Livermorium plasma ($Z=116$), AWBS exactly aligns with the Lorentz gas limit. In the opposite case of the low Z Hydrogen plasma ($Z=1$), the AWBS distribution function approaches significantly the numerical SH solution. BGK takes the Lorentz gas distribution function form for any Z only taking into account the scaling (18).

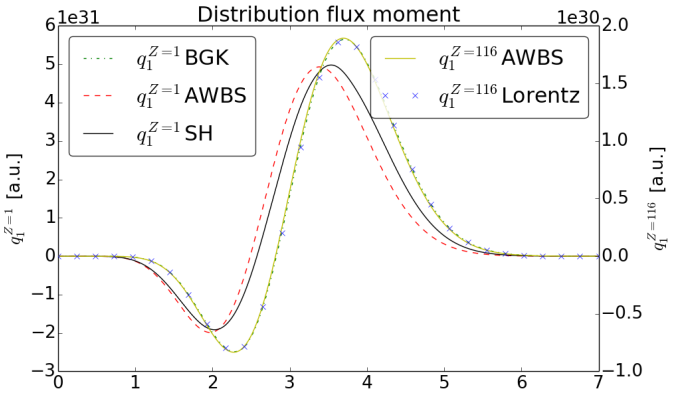

FIG. 1. The flux velocity moment of the anisotropic part of the electron distribution function in low $Z=1$ and high $Z=116$ plasmas in diffusive regime.

It is worth mentioning that the first derivative term in the AWBS collision operator (5) (red dashed line) provides a significant model improvement with respect to the SH (Fokker-Planck) solution (solid black line) compared to the simplest BGK model (8) (dashed-dot blue line) in FIG. 1.

IV. BENCHMARKING THE AWBS NONLOCAL TRANSPORT MODEL

After having shown several encouraging properties of the AWBS transport equation defined by (5) under local diffusive conditions in Sec. III, this section provides a broader analysis of the electron transport and focuses on analysis its behavior under variety of conditions in plasmas. In principle, this is characterized by allowing that electron mean free path can be arbitrarily long, which leads to so-called nonlocal electron transport extensively investigated in numerous publications

[8, 16, 22–26], where the Fokker-Planck modeling of electrons in plasma represents the essential tool. Being so, we introduce our implementation of the AWBS transport equation called AP1, where its results are further benchmarked against simulation results provided by Aladin, Impact VFP codes, and Calder a collisional Particle-In-Cell code. Their description follows in the next section.

A. Implementation of the model

Here, we use the collision operator (5) with (19) and the P1 angular discretization referred to as AP1. It adopts the so-called angular moments method with the electron distribution function having the form

$$\tilde{f} = \frac{f_0}{4\pi} + \frac{3}{4\pi}\boldsymbol{n}\cdot\boldsymbol{f_1}, \tag{20}$$

which consists of the isotropic part represented by the zeroth angular moment $f_0 = \int_{4\pi}\tilde{f}\mathrm{d}\boldsymbol{n}$ and the directional part represented by the first angular moment $\boldsymbol{f_1} = \int_{4\pi}\boldsymbol{n}\tilde{f}\mathrm{d}\boldsymbol{n}$, where $\boldsymbol{n}$ is the transport direction (the solid angle). It should noticed, that (20) represents a multi-dimensional equivalent to (6), where the following relations between the spherical harmonics method and the moments method hold $f^0 = \frac{f_0}{4\pi}$ and $f^1 = \frac{3}{4\pi}|\boldsymbol{f_1}|$.

The first two angular moments applied to the steady form of (1) with collision operator (5) using (19) lead to the AP1 model equations

$$v\frac{\nu_e}{2}\frac{\partial}{\partial v}\left(f_0 - 4\pi f_M\right) = v\nabla\cdot\boldsymbol{f_1} + \frac{q_e}{m_e}\boldsymbol{E}\cdot\left(\frac{\partial\boldsymbol{f_1}}{\partial v} + \frac{2}{v}\boldsymbol{f_1}\right), \tag{21}$$

$$v\frac{\nu_e}{2}\frac{\partial\boldsymbol{f_1}}{\partial v} - \nu_{scat}\boldsymbol{f_1} = \frac{v}{3}\nabla f_0 + \frac{q_e}{m_e}\frac{\boldsymbol{E}}{3}\frac{\partial f_0}{\partial v}, \tag{22}$$

where $\nu_{scat} = \nu_{ei} + \frac{\nu_e}{2}$. The strategy of solving (21) and (22) resides in integrating $\frac{\partial f_0}{\partial v}$ and $\frac{\partial\boldsymbol{f_1}}{\partial v}$ along the velocity magnitude. This is done by starting the integration from infinite velocity ($v = 7v_{th}^{max}$) to zero velocity. The value v_{th}^{max} equals the electron thermal velocity corresponding to the maximum electron temperature in the current profile of plasma. It should be noted, that the backward integration concept is crucial for the model, since it corresponds to the deceleration of electrons due to collisions [27].

1. *Nonlocal electric field treatment*

Similarly to the quasi-neutrality condition (A7), one can obtain the model equation of the electric field $\boldsymbol{E}$ by evaluating the zero current condition (a first moment velocity integration of (22))

$$\int_v\left(\frac{\frac{\nu_e}{2}v^2}{\nu_{scat}}\frac{\partial\boldsymbol{f_1}}{\partial v} - \frac{v^2}{3\nu_{scat}}\nabla f_0 - \frac{v}{3\nu_{scat}}\frac{\partial f_0}{\partial v}\frac{q_e}{m_e}\boldsymbol{E}\right)v^2\,\mathrm{d}v = 0, \tag{23}$$

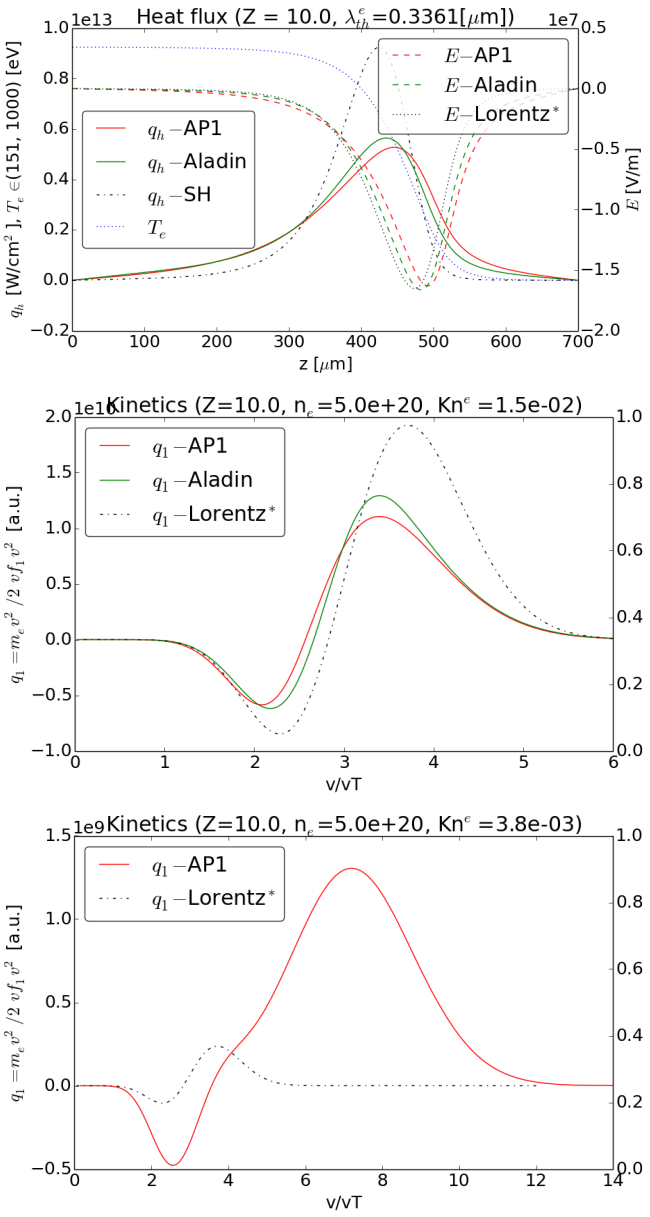

FIG. 2. Snapshot 12 ps. Top: correct steady solution of heat flux. Middle: correct comparison to kinetic profiles at point 442 μm by Aladin. Velocity limit 3.4 v_{th}. Bottom: correct comparison to kinetic profiles at point 550 μm by Aladin. Velocity limit 8.8 v_{th}

from which it is easy to express $\boldsymbol{E}$ once f_0 and $\boldsymbol{f_1}$ are known.

In other words, the integral-differential model equations (21), (22), and (23) need to be solved simultaneously. This is achieved by k-iteration of $f_0^k(\boldsymbol{E}^k)$, $\boldsymbol{f_1}^k(\boldsymbol{E}^k)$, i.e. (21), (22), and $\boldsymbol{E}^{k+1}(f_0^k, \boldsymbol{f_1}^k)$, i.e. (23), until the current evaluation (23) converges to zero. In principle, our concept of k-iteration resembles to the embedded nonlinear iteration of the implicit E field introduced in [12]. The first iteration starts with $\boldsymbol{E} = \boldsymbol{0}$ in (21) and (22)

Kn^e	10^{-4}	10^{-3}	10^{-2}	10^{-1}	1
v_{lim}/v_{th}	70.8	22.4	7.3	3.1	1.8

TABLE II. Scan over varying nonlocality (Kn^e) showing the limit of the collision friction dominance over the acceleration of electrons due to the electric field force. The electric field effect is dominant for electrons with higher velocity than v_{lim} defined in (26). Kn^e and v_{th} are evaluated from the same plasma profiles.

and usually less than 10 iterations is sufficient to obey the quasi-neutrality constraint.

Interestingly, we have encountered a very specific property of the AP1 model with respect to the electric field magnitude. The easiest way how to demonstrate this is to write the model equations (21) and (22) in 1D (z-axis). Then, due to its linear nature, it is easy to eliminate one of the partial derivatives with respect to v, i.e. $\frac{\partial f_0}{\partial v}$ or $\frac{\partial f_{1_z}}{\partial v}$. In the case of elimination of $\frac{\partial f_0}{\partial v}$ one obtains the following equation

$$\left(v\frac{\nu_e}{2}-\frac{2q_e^2E_z^2}{3m_e^2v\nu_e}\right)\frac{\partial f_{1_z}}{\partial v}=\frac{2q_eE_z}{3m_e\nu_e}\frac{\partial f_{1_z}}{\partial z}+\frac{4\pi q_eE_z}{3m_e}\frac{\partial f_M}{\partial v}+\frac{v}{3}\frac{\partial f_0}{\partial z}+\left(\frac{4q_e^2E_z^2}{3m_e^2v^2\nu_e}+\left(\nu_{ei}+\frac{\nu_e}{2}\right)\right)f_{1_z}. \quad (24)$$

It is convenient to write the bracket on the left hand side of (24) as $\frac{2}{3v\nu_e}\left(\left(\sqrt{3}v\frac{\nu_e}{2}\right)^2-\frac{q_e^2}{m_e^2}E_z^2\right)$ from where it is clear that the bracket is negative if $\sqrt{3}v\frac{\nu_e}{2}<\frac{q_e}{m_e}|\boldsymbol{E}|$, i.e. there is a velocity limit for a given magnitude $|\boldsymbol{E}|$, when the collisions are no more fully dominant and the electric field introduces a comparable effect to the collision friction in the electron transport.

It can be shown, that the last term on the right hand side of (24) is dominant and the solution behaves as

$$\Delta\boldsymbol{f_1}\sim\exp\left(\frac{\frac{4q_e^2E_z^2}{3m_e^2v^2\nu_e}+\left(\nu_{ei}+\frac{\nu_e}{2}\right)}{v\frac{\nu_e}{2}-\frac{2q_e^2E_z^2}{3m_e^2v\nu_e}}\Delta v\right), \quad (25)$$

where $\Delta v<0$ represents a velocity step of the implicit Euler numerical integration of decelerating electrons. However, (25) exhibits an exponential growth for velocities above the friction limit (bracket on the left hand side of (24))

$$v_{lim}=\sqrt{\frac{\sqrt{3}\Gamma m_e}{2q_e}\frac{n_e}{|\boldsymbol{E}|}}, \quad (26)$$

which makes the problem to be ill-posed.

In order to provide a stable model, we introduce a reduced electric field to be acting as the accelerating force of electrons

$$|\boldsymbol{E}_{red}|=\sqrt{3}v\frac{m_e}{q_e}\frac{\nu_e}{2}, \quad (27)$$

ensuring that the bracket on the left hand side of (24) remains positive. Further more we define two quantities

$$\omega_{red}=\frac{|\boldsymbol{E}_{red}|}{|\boldsymbol{E}|},\quad \nu_{scat}^E=\frac{q_e}{m_ev}\left(|\boldsymbol{E}|-|\boldsymbol{E}_{red}|\right),$$

introducing the reduction factor of the electric field ω_{red} and the compensation of the electric field effect in terms of scattering ν_{scat}^E. Consequently, the AP1 model (21), (22), and (23) can be formulated as well posed with the help of ω_{red} and ν_{scat}^E. Nevertheless, before doing so, we introduce a slightly different approximation to the electron distribution function as

$$\tilde{f}=\frac{4\pi f_M+\delta f_0}{4\pi}+\frac{3}{4\pi}\boldsymbol{n}\cdot\boldsymbol{f_1}. \quad (28)$$

where δf_0 represents the departure of isotropic part from the Maxwell-Boltzmann equilibrium distribution f_M. Then, the stable AP1 model reads

$$v\frac{\nu_e}{2}\frac{\partial\delta f_0}{\partial v}=v\nabla\cdot\boldsymbol{f_1}+\frac{q_e}{m_e}\boldsymbol{E}\cdot\left(\omega_{red}\frac{\partial\boldsymbol{f_1}}{\partial v}+\frac{2}{v}\boldsymbol{f_1}\right), \quad (29)$$

$$v\frac{\nu_e}{2}\frac{\partial\boldsymbol{f_1}}{\partial v}=\tilde{\nu}_{scat}\boldsymbol{f_1}+\frac{v}{3}\nabla\left(4\pi f_M+\delta f_0\right)+\frac{q_e\boldsymbol{E}}{3m_e}\left(4\pi\frac{\partial f_M}{\partial v}+\omega_{red}\frac{\partial\delta f_0}{\partial v}\right), \quad (30)$$

where $\tilde{\nu}_{scat}=\nu_{ei}+\nu_{scat}^E+\frac{\nu_e}{2}$.

The reason for keeping f_M in the distribution function approximation (28) can be seen in the last term on the right hand side of (30), which provides the effect of electric field on directional quantities as current or heat flux. In principle, the explicit use of f_M ensures the proper effect of $\boldsymbol{E}$ if $\delta f_0\ll f_M$, i.e. no matter what the reduction ω_{red} is. Apart from its stability, it also exhibits much better convergence of the electric field, which is now given by the zero current condition of (30) as

$$\boldsymbol{E}=\frac{\int_v\left(\frac{\nu_e}{2\tilde{\nu}_{scat}}v^2\frac{\partial\boldsymbol{f_1}}{\partial v}-\frac{v^2}{3\tilde{\nu}_{scat}}\nabla\left(4\pi f_M+\delta f_0\right)\right)v^2\,\mathrm{d}v}{\frac{q_e}{m_e}\int_v\frac{v}{3\tilde{\nu}_{scat}}\left(4\pi\frac{\partial f_M}{\partial v}+\omega_{red}\frac{\partial\delta f_0}{\partial v}\right)v^2\,\mathrm{d}v}. \quad (31)$$

For practical reasons we present in TABLE II some explicit values of velocity limit corresponding to varying transport conditions expressed in terms of "Z" Knudsen number $\mathrm{Kn}^e=\frac{\lambda_e}{\sqrt{Z+1}L_{T_e}}$, where $\sqrt{Z+1}$ provides a proper scaling of nonlocality with respect to ionization, i.e. the effect of scattering of electrons on ions [24].

B. Aladin, Impact, and Calder kinetic codes

- Brief description of the Aladin code FIG. 4, FIG. 2.
- Brief description of the Calder code FIG. 3.

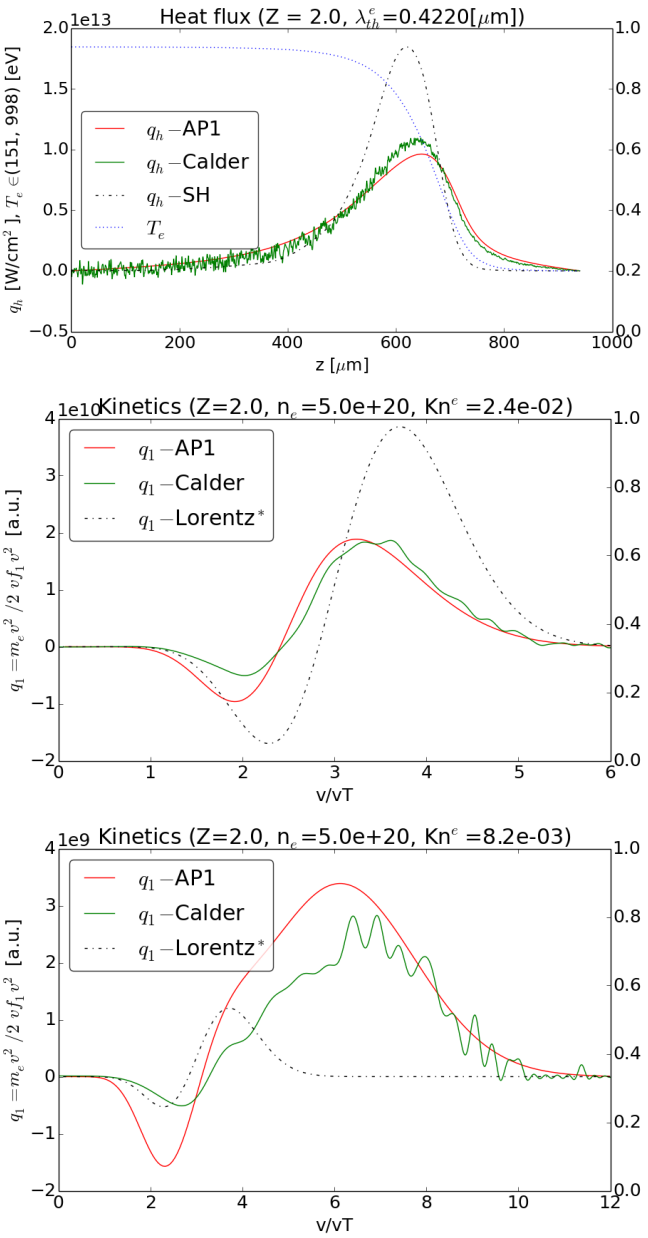

FIG. 3. Snapshot 11 ps. Left: correct steady solution of heat flux. Velocity limit 6.4 v_{th}.

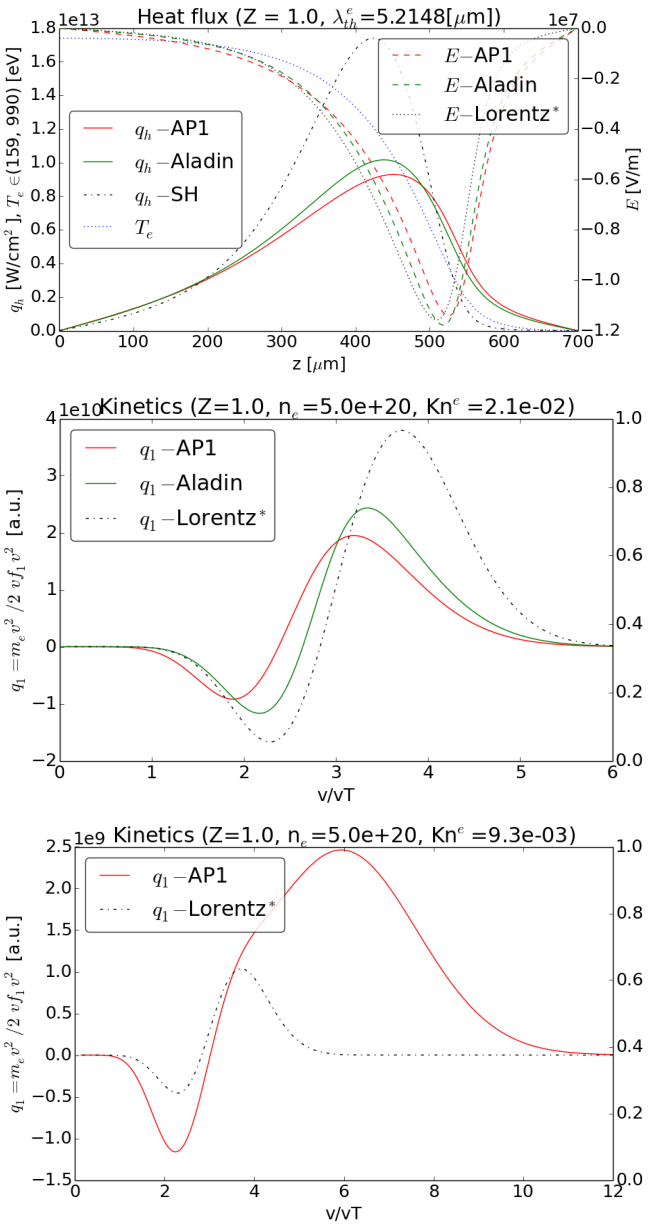

FIG. 4. Snapshot 20 ps. Top: correct steady solution of heat flux. Right: Aladins results are correct. Velocity limit 4.4 v_{th}. Snapshot 20 ps. AP1 kinetic profiles at point 580 μm corresponding to a highly nonlocal nature of the heat flux and is in a good agreement with [29]. Velocity $max(q_1) = 6.0\ v_{th}$. Velocity limit 9.0 v_{th}.

C. Tests relevant to laser-heated plasmas

Among a variety of test suitable for benchmarking the nonlocal electron transport models published [16, 17, 21, 28–30], we decided to focus on conditions relevant to inertial confinement fusion plasmas generated by lasers.

1. *Heat-bath problem*

The accuracy of the AP1 implementation is compared to Aladin, Impact and Calder codes by calculating the heat flow in the case where a large relative temperature variation

$$T_e(z) = 0.575 - 0.425 \tanh\left((z - 450)s\right), \qquad (32)$$

which exhibits a smooth steep gradient at point 450 μm connecting a hot bath ($T_e = 1$ keV) and cold bath ($T_e = 0.17$ keV) and s is the parameter of steepness. This test is referred to as a simple non-linear heat-bath problem and originally was introduced in [28] and further investigated in [16, 17, 29, 30].

The total computational box size is 700 μm in the case of Aladin and Impact and 1000 μm in the case of Calder. We performed Aladin, Impact, and Calder simulations showing an evolution of temperature starting from the initial profile (32). Due to an inexact initial distribution function (approximated by Maxwellian), the first phase of the simulation exhibits a transient behavior of the heat flux. After several ps the distribution adjusts properly to its nonlocal nature and the actual heat flux profile can be compared. We then take the temperature profile from Aladin/Impact/Calder and used our AP1 implementation to calculate the heat flow it would predict given this profile. In particular, the AP1 results corresponding to the evolved temperature profile by Aladin can be found in FIG. 4 and FIG. 2 for $Z = 1$ and $Z = 10$ respectively. The AP1 results computed on the evolved temperature profile for $Z = 2$ by Calder can be found in FIG. 3.

For all heat-bath simulations the electron density, Coulomb logarithm and ionisation were kept constant and uniform. The coulomb logarithm was held fixed throughout, $\ln\Lambda = 7.09$. Nevertheless, the Knudsen number Kn^e has been varied among the simulation runs in order to address a broad range of nonlocality of the electron transport corresponding to the laser-heated plasma conditions, i.e. $\mathrm{Kn}^e \in (0.0001, 1)$. The variation of Kn^e arises from the variation of the uniform electron density $n_e \in (10^{19}, 10^{23})$ cm^{-3} or the length scale given by the slope of the temperature profile $s \in (1/2500, 1/25)\mu$m. Results of an extensive set of simulations of varying Kn^e is shown in FIG. 5.

Apart from the distribution function details related to the point of the heat flux maximum, in FIG. 4 we also present the detail of the kinetic profile at point 580 μm corresponding to a highly nonlocal nature of the heat flux profile. Here a good agreement with [29] can be found.

In every simulation run of AP1 we used 250 velocity groups in order to avoid numerical errors in modeling of the electron kinetics. However, a smaller number of groups, e.g. 50, provides a very similar results (an error around 10% in the heat flux).

2. *Hohlraum problem*

Additionally to the steep temperature gradients, the laser-heated plasma experiments also involve steep density gradients and variation in ionization, which is even more dominant in multi-material targets as in inertial fusion experiments, e.g. at the interface between the helium gas-fill and the ablated high Z plasma.

In [30], a kinetic simulation of such a test was introduced. Plasma profiles provided by a HYDRA simulation in 1D spherical geometry of a laser-heated gadolinium hohlraum containing a typical helium gas-fill were used as input for the IMPACT [12] VFP code. Electron temperature T_e, electron density n_e and ionisation Z profiles shown in FIG. 6 at 20 nanoseconds of the HYDRA simulation were used (after spline smoothing) as the initial conditions for the IMPACT run (in planar geometry). For simplicity, the Coulomb logarithm was treated as a constant $\ln\Lambda_{ei} = \ln\Lambda_{ee} = 2.1484$. In reality, in the low-density corona $\ln\Lambda$ reaches 8, which, however, does not affect the heat flux profile significantly.

It is worth mentioning that in the surroundings of the heat flux maximum ($\sim 1662\mu$m) the profiles of all plasma variables exhibit steep gradients with a change from $T_e = 2.5$ keV, $n_e = 5{\times}10^{20}$ cm^3, $Z = 2$ to $T_e = 0.3$ keV, $n_e = 6{\times}10^{21}$ cm^3 , $Z = 44$ across approximately 100 μm (between 1600 μm and 1700 μm), starting at the helium-gadolinium interface.

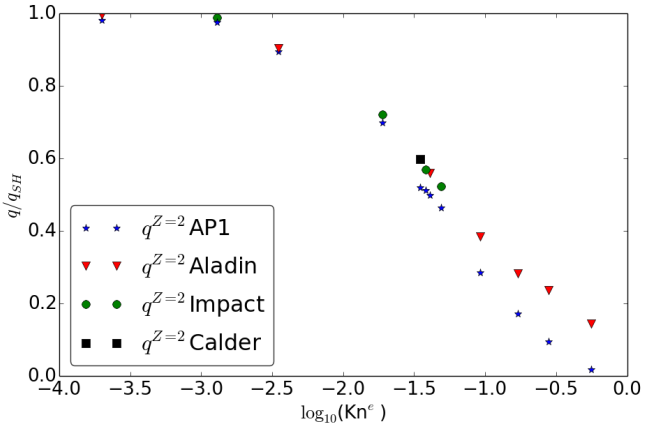

FIG. 5. Simulation results for the case $Z = 2$ computed by AP1/Aladin/Impact/Calder. Every point corresponds to the maximum heat flux in a "tanh" temperature simulation, which can be characterized by Kn. The range of $\log_{10}(\mathrm{Kn}) \in (0, -4)$ can be expressed as equivalent to the electron density approximate range $\mathrm{n}_e \in (1e19, 3.5e22)$ of the 50 μm slope tanh case. In the case of $\mathrm{Kn} = 0.56$, $q_{Aladin}/q_{AP1} \approx 7.9$.

V. CONCLUSIONS

- The most important point is that we introduce a collision operator, which is coherent with the full FP, i.e. no extra dependence on Z.
- Touch pros/contras of linearized FP in Aladin and Impact vs AWBS
- Raise discussion about what is the weakest point of AP1 for high Kns: the velocity limit or phenomenological Maxwellization?

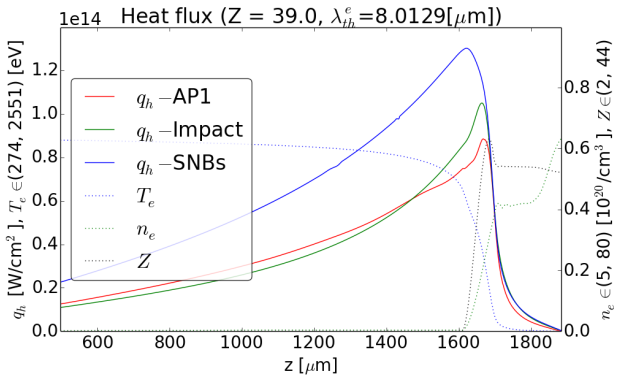

FIG. 6.

- Summarize useful outcomes related to plasma physics as the tendency of the velocity maximum in q_1 with respect to Z and Kn^e.
- Emphasize the good results of Aladin (compared to Impact) and also outstanding results of Calder while being PIC.

ACKNOWLEDGMENTS

Appendix A: Background of the local diffusive regime theory

The left hand side of (7) acts on (6) as

$$\mu\left(\frac{\partial\tilde{f}}{\partial z}+\frac{q_eE_z}{m_ev}\frac{\partial\tilde{f}}{\partial v}\right)+\frac{q_eE_z}{m_e}\frac{1-\mu^2}{v^2}\frac{\partial\tilde{f}}{\partial\mu}= \mu\left(\frac{\partial f^0}{\partial z}+\frac{q_eE_z}{m_ev}\frac{\partial f^0}{\partial v}\right)+\frac{q_eE_z}{m_ev^2}f^1+O(\mu^2). \quad \text{(A1)}$$

The action on (6) of the BGK operator (8) as used in (7) reads

$$\frac{1}{v}C_{BGK}(\tilde{f})=\frac{\tilde{f}-f_M}{\lambda_e}+\frac{1}{2}\left(\frac{Z}{\lambda_e}+\frac{1}{\lambda_e}\right)\frac{\partial}{\partial\mu}(1-\mu^2)\frac{\partial\tilde{f}}{\partial\mu}, =\frac{f^0-f_M}{\lambda_e}-\mu\frac{Z}{\lambda_e}f^1. \quad \text{(A2)}$$

Consequently, if the isotropic and anisotropic parts of (A1) and (A2) are compared, one finds the following equations

$$f^0=f_M+\frac{\lambda_eq_eE_z}{m_ev^2}f^1, \quad \text{(A3)}$$

$$f^1=-\frac{\lambda_e}{Z}\left(\frac{\partial f^0}{\partial z}+\frac{q_eE_z}{m_ev}\frac{\partial f^0}{\partial v}\right). \quad \text{(A4)}$$

It is valid to assume that $f^0=f_M$ from (A3). Then,

$$f^1_{BGK}=-\frac{\lambda_e}{Z}\left(\frac{\partial f_M}{\partial z}+\frac{q_eE_z}{m_ev}\frac{\partial f_M}{\partial v}\right). \quad \text{(A5)}$$

The *quasi-neutrality* constraint, corresponding to a zero electric reads

$$\boldsymbol{j}\equiv q_e\int\boldsymbol{v}\tilde{f}\,\mathrm{d}\boldsymbol{v}=\boldsymbol{0}. \quad \text{(A6)}$$

In the case of the BGK EDF, in particular its anisotropic part (A5), the zero current condition takes the form

$$2\pi\int_{-1}^{1}\int_v v\mu^2f^1_{BGK}\,\mathrm{d}v\mathrm{d}\mu=0,$$

which leads to the electric field (same as the classical Lorentz electric field [20])

$$E_z=\frac{m_ev_{th}^2}{q_e}\left(\frac{1}{L_{n_e}}+\frac{5}{2}\frac{1}{L_{T_e}}\right). \quad \text{(A7)}$$

It is worth mentioning, that the deviation of f^0 from f_M in (A3) can be written as $\left(\frac{\lambda_e}{L_{n_e}}+\frac{5}{2}\frac{\lambda_e}{L_{T_e}}\right)\frac{v_{th}^2}{v^2}f^1$, where naturally arises the Knudsen number $Kn=\frac{\lambda_e}{L_{n_e}}+\frac{5}{2}\frac{\lambda_e}{L_{T_e}}$ comprising both contributions of electron density and temperature gradients.

In the case of the AWBS operator (5) used in (7), its action on (6) reads

$$\frac{1}{v}C_{AWBS}(\tilde{f})=\frac{v}{\lambda_e}\frac{\partial}{\partial v}\left(\tilde{f}-f_M\right) +\frac{1}{2}\left(\frac{Z}{\lambda_e}+\frac{1}{\lambda_e}\right)\frac{\partial}{\partial\mu}(1-\mu^2)\frac{\partial\tilde{f}}{\partial\mu} =\frac{v}{\lambda_e}\frac{\partial}{\partial v}\left(f^0-f_M\right) +\mu\left(\frac{v}{\lambda_e}\frac{\partial f^1}{\partial v}-\frac{Z+1}{\lambda_e}f^1\right). \quad \text{(A8)}$$

One finds the following equations if the isotropic and anisotropic parts of (A1) and (A8) are compared

$$\frac{\partial}{\partial v}\left(f^0-f_M\right)=\frac{\lambda_eq_eE_z}{m_ev^2}\frac{f^1}{v}, \quad \text{(A9)}$$

$$\frac{v}{\lambda_e}\frac{\partial f^1}{\partial v}-\frac{Z+1}{\lambda_e}f^1=\frac{\partial f^0}{\partial z}+\frac{q_eE_z}{m_ev}\frac{\partial f^0}{\partial v}. \quad \text{(A10)}$$

If we assume that $\frac{\partial f^0}{\partial v}=\frac{\partial f_M}{\partial v}$, i.e. $f^0=f_M$, the anisotropic part of the AWBS operator is governed by the equation

$$\frac{\partial f^1_{AWBS}}{\partial v}-\frac{Z+1}{v}f^1_{AWBS}=\frac{\lambda_e}{v}\left(\frac{\partial f_M}{\partial z}+\frac{q_eE_z}{m_ev}\frac{\partial f_M}{\partial v}\right). \quad \text{(A11)}$$

Even though it is not straightforward, the electric field in (A11) (solved numerically) providing a zero current exactly matches (A7). Consequently, the deviation of $\frac{\partial f^0}{\partial v}$ from $\frac{\partial f_M}{\partial v}$ in (A9) can be written as $Kn\frac{v_{th}^2}{v^2}\frac{f^1}{v}$.

Finally, it should be stressed, that the concept of locality expressed as $Kn\ll 1$ is crucial for our *local diffusive regime* analysis, because it provides sufficient Maxwellization, i.e. (A3) and (A9), and correspondingly, (A5) and (A11) are valid models.

[1] R. S. Cohen, L. Spitzer, Jr., P. M. Routly, The electrical conductivity of an ionized gas, Phys. Rev. 80 (1950) 230–238.

[2] J. H. Jeans, Astronomy and Cosmogony, Cambridge University Press, London, 1929.

[3] S. Chandrasekhar, Stochastic problems in physics and astronomy, Rev. Mod. Phys. 15 (1943) 1.

[4] M. Planck, Über einen Satz der statistischen Dynamik und seine Erweiterung in der Quantentheorie, Sitzungsber. Preuss. Akad. Wiss. 24 (1917) 324–341.

[5] L. Spitzer, Jr. and R. Härm, Transport phenomena in a completely ionized gas, Phys. Rev. 89 (1953) 977.

[6] J. H. Jeans, The equations of radiative transfer of energy, Month. Not. Royal Astr. Soc. 78 (1917) 28–36.

[7] M. N. Rosenbluth, W. M. MacDonald, D. L. Judd, Fokker-planck equation for an inverse-square force, Phys. Rev. 107 (1957) 1.

[8] A. R. Bell, R. G. Evans, D. J. Nicholas, Phys. Rev. Lett. 46 (1981) 243.

[9] J. P. Matte, J. Virmont, Electron heat transport down steep temperature gradients, Phys. Rev. Lett. 49 (1982) 1936–1939.

[10] S. I. Braginskii, Transport processes in a plasma, Reviews of Plasma Physics 1 (1965) 205.

[11] J. R. Albritton, E. A. Williams, I. B. Bernstein, K. P. Swartz, Nonlocal electron heat transport by not quite maxwell-boltzmann distributions, Phys. Rev. Lett. 57 (1986) 1887–1890.

[12] R. J. Kingham, A. R. Bell, An implicit Vlasov-Fokker-Planck code to model non-local electron transport in 2-D with magnetic fields, J. Comput. Phys. 194 (194) (2004) 1–34.

[13] F. Perez, L. Gremillet, A. Decoster, M. Drouin, E. Lefebvre, Improved modeling of relativistic collisions and collisional ionization in particle-in-cell codes, Phys. Plasmas 19 (2012) 083104.

[14] L. Landau, Kinetic equation for the coulomb effect, Phys. Z. Sowjetunion 10 (1936) 154.

[15] N. J. Fish, Theory of current drive in plasmas, Rev. Mod. Phys. 59 (1987) 175.

[16] D. D. Sorbo, J.-L. Feugeas, P. Nicolai, M. Olazabal-Loume, B. Dubroca, S. Guisset, M. Touati, V. Tikhonchuk, Reduced entropic model for studies of multidimensional nonlocal transport in high-energy-density plasmas, Phys. Plasmas 22 (2015) 082706.

[17] D. D. Sorbo, J.-L. Feugeas, P. Nicolai, M. Olazabal-Loume, B. Dubroca, V. Tikhonchuk, Extension of a reduced entropic model of electron transport to magnetized nonlocal regimes of high-energy-density plasmas, Laser Part. Beams 34 (2016) 412–425.

[18] P. Bhatnagar, E. Gross, M. Krook, A Model for Collision Processes in Gases. I. Small Amplitude Processes in Charged and Neutral One-Component Systems, Phys. Rev. 94 (1954) 511–525.

[19] I. P. Shkarofsky, T. W. Johnston, M. P. Bachynskii, The particle Kinetics of Plasmas, Addison-Wesley, Reading, 1966.

[20] H. A. Lorentz, The motion of electrons in metallic bodies, in: Proceedings of the Royal Netherlands Academy of Arts and Sciences, Amsterdam, Vol. 7, 1905, pp. 438–453.

[21] E. M. Epperlein, R. W. Short, A practical nonlocal model for electron heat transport in laser plasmas, Phys. Fluids B 3 (1991) 3092–3098.

[22] R. C. Malone, R. L. McCroy, R. L. Morse, Phys. Rev. Lett. 34 (1975) 721.

[23] D. G. Colombant, W. M. Manheimer, M. Busquet, Test of models for electron transport in laser produced plasmas, Phys. Plasmas 12 (2005) 072702.

[24] J. F. Luciani, P. Mora, J. Virmont, Nonlocal heat transport due to steep temeperature gradients, Phys. Rev. Lett. 51 (1983) 1664–1667.

[25] A. V. Brantov, V. Y. Bychenkov, V. T. Tikhonchuk, Nonlocal electron transport in laser heated plasmas, Phys. Plasmas 5 (1998) 2742–2753.

[26] G. Schurtz, P. Nicolai, M. Busquet, A nonlocal electron conduction model for multidimensional radiation hydrodynamics codes, Phys. Plasmas 4238 (2000) 7.

[27] M. Touati, J.-L. Feugeas, P. Nicolai, J. Santos, L. Gremillet, V. Tikhonchuk, A reduced model for relativistic electron beam transport in solids and dense plasmas, New J. Phys. 16 (2014) 073014.

[28] A. Marocchino and M. Tzoufras and S. Atzeni and A. Schiavi and Ph. Nicolai and J. Mallet and V. Tikhonchuk and J.-L. Feugeas, Comparison for non-local hydrodynamic thermal conduction models, Phys. Plasmas 20 (2013) 022702.

[29] M. Sherlock, J. P. Brodrick, C. P. Ridgers, A comparison of non-local electron transport models for laser-plasmas relevant to inertial confienement fusion, Phys. Plasmas 24 (2017) 082706.

[30] J. P. Brodrick, R. J. Kingham, M. M. Marinak, M. V. Patel, A. V. Chankin, J. T. Omotani, M. V. Umansky, D. D. Sorbo, B. Dudson, J. T. Parker, G. D. Kerbel, M. Sherlock, C. P. Ridgers, Testing nonlocal models of electron thermal conduction for magnetic and inertial confinement fusion applications, Phys. Plasmas 24 (2017) 092309.